

The metal-rich globular clusters of the Milky Way

F. Heitsch¹ and T. Richtler²

¹ Max-Planck-Institut für Astronomie, Königstuhl 17, 63119 Heidelberg, Germany

² Sternwarte der Universität Bonn, Auf dem Hügel 71, 53115 Bonn, Germany

Received / Accepted

Abstract. We present new (V,V-I)-photometry of the metal-rich globular clusters NGC 5927, 6316, 6342, 6441 and 6760. The clusters show differential reddening up to $\delta E_{V-I} = 0.32$ mag, for which the CMDs are corrected via extinction maps. There are hints of a variation in the extinction law. Two different ways to determine the parameters metallicity, reddening and distance lead to consistent results. The metallicities of the clusters range between $-0.7 \leq [M/H] \leq 0.0$ dex and the absolute reddening between $0.43 \leq E_{V-I} \leq 0.76$ mag. Taking the differential reddening into account leads to slightly increased distances. From the resulting parameters we conclude that the usual halo-disk-distinction in the system of globular clusters seems questionable.

Key words: Galaxy: center – globular clusters: general – Galaxy: structure

1. Introduction

The globular cluster system of the inner Milky Way is still not well understood. This is particularly true for the clusters' classification with respect of the galactic population structure. Because reliably determined parameters, e.g. metallicity, reddening, distance and age, are the basic requirement of any discussion, we present new photometry in (V, I) of the metal-rich globular clusters (GC's) NGC 5927, 6316, 6342, 6441 and 6760. We also re-discuss NGC 6528 and NGC 6553, where the data have already been published (Richtler et al. 1998, Sagar et al. 1998).

As there has been evidence for a correlation between metallicity and spatial distribution of the GC's since the late 1950's, Zinn (1985) classified the clusters via their kinematics, spatial distribution and metallicity into two subsystems: The disk-system with clusters of metallicity $[M/H] \geq -0.8$ dex and the halo-system with $[M/H] \leq -0.8$ dex. The disk-system shows a high rotational velocity and a small velocity dispersion, the halo-system vice versa. Armandroff (1989) derived a scale height of 1.1 kpc

for the disk-system, which he identified with the galactic thick disk via rotational velocities and velocity dispersions. By comparing the metal-rich GC's of the inner 3 kpc with the underlying stellar population, Minniti (1995) assigned these objects to the bulge rather than to the disk. Burkert & Smith (1997) used kinematical arguments and the masses of the clusters to divide the metal-rich subsystem of Zinn (1985) into a bulge, a bar and a disk-group.

The thing these subdivisions have in common is, that they refer to the entire system of clusters and they try to formulate their criteria by identifying subsystems within the whole system. For the other way around, i.e. to classify observed objects with any of these subgroups, accurate parameters are needed. The halo clusters are well discernible from any other subsystem, but the metal-rich clusters near the galactic center are not. The determination of their parameters encounters observational difficulties, as their low galactic latitudes lead to strong contamination with field stars and to strong (differential) reddening. These effects have to be taken care of.

There is a variety of photometry existing for the program clusters. Recent studies on NGC 5927 were done by Fullton et al. (1996) and Samus et al. (1996). Armandroff (1988) presented and discussed CMDs including NGC 6316, 6342 and 6760. There is a photometry of NGC 6441 in (B,V) of Hesser & Hartwick (1976) and a more recent one in Rich et al. (1997). CMDs of NGC 6528 have been discussed by Ortolani et al. (1990) and Richtler et al. (1998). Guarnieri et al. (1998) as well as Sagar et al. (1998) present (V,I)-photometry of NGC 6553. Zinn (1985), Armandroff (1989), Richtler et al. (1994), Minniti (1995) and Burkert & Smith (1997) discuss the subdivision of the GC-system into a halo, disk and/or bulge component.

As the data and their reduction shall be published in a forthcoming paper, section 2 deals only briefly with this subject. In section 3 and 4, the derived CMDs are presented and the effects of differential reddening are discussed and removed. Section 5 contains the methods and results of the parameter determination, and in section 6 we will discuss the resulting classification and its problems.

2. Observations and reduction

The observations in V and I were carried out at La Silla/Chile between July 16th and 19th 1993. We used the 2.2m with CCD ESO #19, which covers with 1024×1024 pix an area of $5.7' \times 5.7'$ on the sky. The seeing was $1.1''$. In addition to the ground-based data, we used data of the Hubble-Space-Telescope (HST) for NGC 5927. These data have already been published by Fullton et al. (1996).

To reduce the data, we used the DAOPHOT-package (Stetson 1987, 1992), together with the ESO-MIDAS-system (version 1996). The calibrating equations (1), determined via Landolt standard stars (Landolt 1992), are

$$\begin{aligned} V_{st} &= V_{inst} - (1.38 \pm 0.05) + (0.057 \pm 0.003)(V - I)_{st} \\ I_{st} &= I_{inst} - (2.62 \pm 0.05) - (0.060 \pm 0.003)(V - I)_{st} \end{aligned} \quad (1)$$

Together with the error of the photometry and of the PSF-aperture-shift, we get an absolute error for a single measurement of ± 0.06 mag. For a more extensive treatment of the data and their reduction, see Heitsch & Richtler (1999). To calibrate the HST-data, we used the relations and coefficients as described by Holtzman (1995). In agreement with Guarnieri et al. (1998), we detected a systematic shift between calibrated ground-based and HST-magnitudes of about 0.2 mag with the HST-magnitudes being fainter. This difference might be due to crowding influences on the calibration stars in the ESO-frame, as explained by Guarnieri et al.

3. Colour-Magnitude-Diagrams

3.1. NGC 5927

The unselected CMD for NGC 5927 is shown in Fig. 6. The cluster's HB and RGB are clearly distinguishable, with the HB overlapping the RGB, as well as the stars of some field population to the blue of the cluster's structures covering the TOP-region. Some 0.5 mag below the HB, the RGB-bump is discernible. The elongation of the HB and the broadening of the RGB are due to differential reddening, as we now argue. As the HB of metal-rich GCs generally is rather clumped and the HB-stars all have the same luminosity, differential reddening should cause an elongation of the HB parallel to the reddening vector.

Fig. 2 shows the coordinates of the radially selected cluster stars with special markings for the HB-stars as given by Fig. 1. If differential reddening is indeed responsible for the observed elongation, we do not expect to find any red faint stars in areas where blue bright stars are to be found, unless the reddening is very (!) patchy. In the case of NGC 5927, we note (Fig. 2) that the blue bright stars are located in an area west of the cluster's center, and thus differential reddening is indeed responsible for the elongated HB structure.

In Fig. 20 we present the calibrated HST-CMDs of NGC 5927. They all show a slightly broadened lower RGB

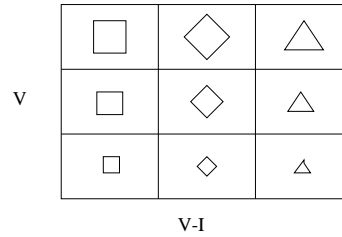


Fig. 1. Symbols for brightness and colour of the HB-stars in diagrams 2 to 5. With the box covering the HB-region of a cluster, all the stars in one of the nine subfields are denoted by the corresponding symbol. Increasing symbol size denotes increasing brightness. Increasing colour-index is represented by a change from squares to lozenges to triangles.

as well as a slightly tilted HB. The TOP is well resolved. However, the CMDs do not extend to the bright stars of the AGB/RGB due to pixel overflow on the exposures. As mentioned above, the HST-CMDs are shifted with respect to the ESO-CMDs to fainter magnitudes. Richtler et al. (1998) argue that the ground-based calibration is not erroneous. Thus, we will use the ground-based calibrated data for the further analysis. For a detailed discussion see Heitsch & Richtler (1999).

3.2. NGC 6316

The unselected CMD (Fig. 8) shows beside the cluster a strong contribution from the field population. The field main sequence is striking. The cluster RGB is broadened, but since the clumpy HB indicates only small differential reddening, the RGB width is probably to a large part due to the field contamination. Determining a correlation between HB-stars and coordinates as in Fig. 2 led to no convincing results, because the field does not contain enough stars.

3.3. NGC 6342

NGC 6342 (Fig. 10) shows a sparsely populated AGB/RGB due to the small size of the cluster. The TOP-region and upper MS are reached. Fig. 3 gives the location of HB-stars as in Fig. 2. Blue, bright HB-stars are to be found in an area to the south of the cluster's center.

3.4. NGC 6441

NGC 6441 (Fig. 12) is located behind a dense field population, the stars of which can be found between $1.0 \leq V - I \leq 1.5$ mag. This population covers the lower part of the RGB of NGC 6441 as well. Its TOP is not reached. We mention some special features. First, we find some stars between $1.8 \leq V - I \leq 2.0$ mag and above the HB of NGC 6441. These could be HB-stars of a population which is similar to NGC 6441 and is located between the

cluster and ourselves, as the stars are shifted in V only. In this case, we would have to assume that the absolute reddening is caused by some cloud between this population and the observer. Otherwise it would have to be shifted in $V - I$ as well. Second, we find some stars to the blue of the clumpy, tilted HB of NGC 6441. These stars seemingly belong to the cluster, as they are still visible when selecting for small radii. Probably they belong to the blue HB of NGC 6441, which has been discovered by Rich et al. (1997). The difference in star density (Fig. 4) is due to the fact that the calibration exposures were shifted by around 360 pix to the south. Taking this into account, we find that the blue bright stars are mostly found in the western two thirds of the cluster.

3.5. NGC 6760

Fig. 14 not only shows the already discussed structures such as HB, RGB and field population, but it shows the RGB-bump below the HB as well. The RGB is rather broadened. The HB and RGB-bumps are elongated and tilted with the same slope. The HB-stars, marked according to colour and brightness, are found in Fig. 5.

3.6. NGC 6528 and NGC 6553

The CMDs for NGC 6528 and 6553 (Fig. 16, 18) have already been published (Richtler et al. 1998, Sagar et al. 1998). As described in their papers, NGC 6528 not only shows a broadened RGB and a tilted and elongated HB, but it shows also some background population below the AGB/RGB. The field population covers the TOP-region of the cluster. Moreover, the RGB-bump of NGC 6528 is clearly visible some 0.5 mag below the HB. The CMD of NGC 6553 shows the same characteristics as NGC 6528, however they are even more distinct. Here we clearly see the background population with its RGB and AGB/RGB strongly differentially reddened.

4. Correction for differential reddening

In order to correct the CMDs for differential reddening, we used a refined version of the method described by Grebel et al. (1995). The entire frame is divided into subframes. These are determined by covering the whole frame with a regular subgrid and dividing the grid cells further until the number of stars in one cell becomes too small to define the CMD structure. The CMDs will be shifted according to the reddening vector (described below) with respect to CMDs from neighbouring cells. The shift in colour supplies the differential reddening. If two neighbouring subframes have the same reddening, these subframes are merged. There are two problems with this method: First, one has to be careful to use the HB as a means for comparing two CMDs, as the HB may be intrinsically elongated. Useful results can only be achieved by comparing the RGBs and

TOPs, as far as they are accessible. Second, the size of the subfields must be large enough to render meaningful CMDs. Fig. 22 shows the resulting extinction maps for the seven clusters. The smallest subfields have a size of about $28'' \times 28''$. But as some of them still showed differential reddening, the scale of the structures responsible for the differential reddening is expected to be even smaller. The smallest scales we got from a comparison of coordinates of stars with different reddening amounted to values of $4''$.

For the correction of the CMDs we need the extinction

$$A_V = R_V^B E_{B-V} = R_V^I E_{V-I}. \quad (2)$$

However, assuming a uniform reddening law led to CMDs which in some cases showed the corrected HBs having larger or smaller slopes than the uncorrected HBs. Moreover, as there is some uncertainty in the literature regarding R_V^B , with values varying between $R_V^B = 3.1$ (Savage & Mathis 1979) and $R_V^B = 3.6$ (Grebel & Roberts 1995), we determined the slope of the reddening vector via the tilted HBs of our CMDs. This leads to reasonable results only if the HBs are intrinsically clumpy. This assumption is corroborated by the fact that the well dereddened CMDs (Fig. 23, 27, 29) have clumpy HBs indeed. Table 1 shows the slopes R_V^I for each cluster. In Fig. 21, the slopes are plotted against the galactic longitude. These variations, although at the margin of the errors, confirm earlier observations by Meyer & Savage (1981) and Turner (1994). Meyer & Savage determined via two-color-diagrams the deviation of single stars in the extinction behaviour from the galactic mean extinction law. Turner demonstrated the inapplicability of a mean galactic reddening law for objects lying close to the galactic plane. To correct the

NGC	ΔE_{V-I}^{max}	R_V^I
5927	0.27	1.9 ± 0.2
6316	0.07	2.1 ± 0.2
6342	0.32	2.2 ± 0.1
6441	0.20	2.3 ± 0.1
6760	0.25	2.0 ± 0.1
6528	0.31	2.4 ± 0.3
6553	0.29	2.3 ± 0.2

Table 1. Maximum differential reddening and slope of the reddening vector.

diagrams for differential reddening, we referred all sub-CMDs of one cluster to the one with detected minimal reddening and we shifted all other sub-CMDs onto that. As we thus use the minimal absolute reddening as a point of reference, the absolute reddening determined later on will be smaller than value given in the literature. The differentially dereddened CMDs are shown in Figs. 7 through 19. As the correction led to a clearly improved appearance

for all clusters, the corrected versions of the CMDs will be used for further investigation.

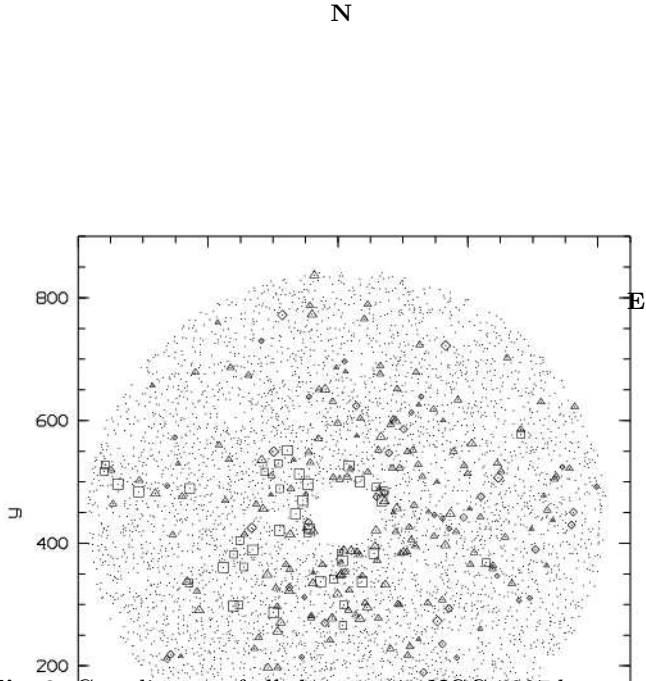


Fig. 2. Coordinates of all the stars in NGC 5927 between $50 \leq r \leq 400$ pix, r being the distance to the cluster's center in pixel. The HB-stars are marked according to Fig. 1. Blue bright stars are to be found in an area $0 \leq x < 500$ pix and $250 \leq y \leq 575$ pix. The stars are selected for photometric errors ≤ 0.03 mag.

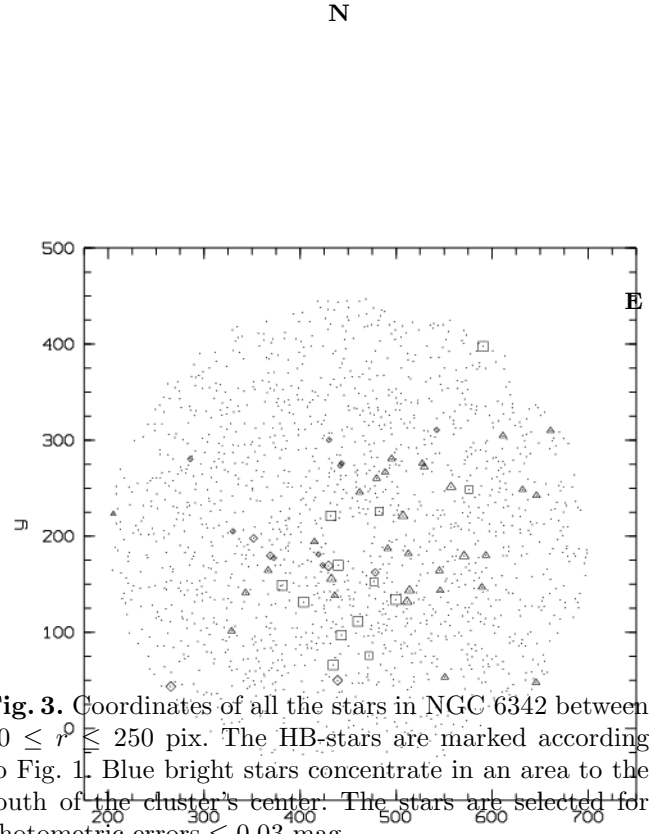


Fig. 3. Coordinates of all the stars in NGC 6342 between $30 \leq r \leq 250$ pix. The HB-stars are marked according to Fig. 1. Blue bright stars concentrate in an area to the south of the cluster's center. The stars are selected for photometric errors ≤ 0.03 mag. \times

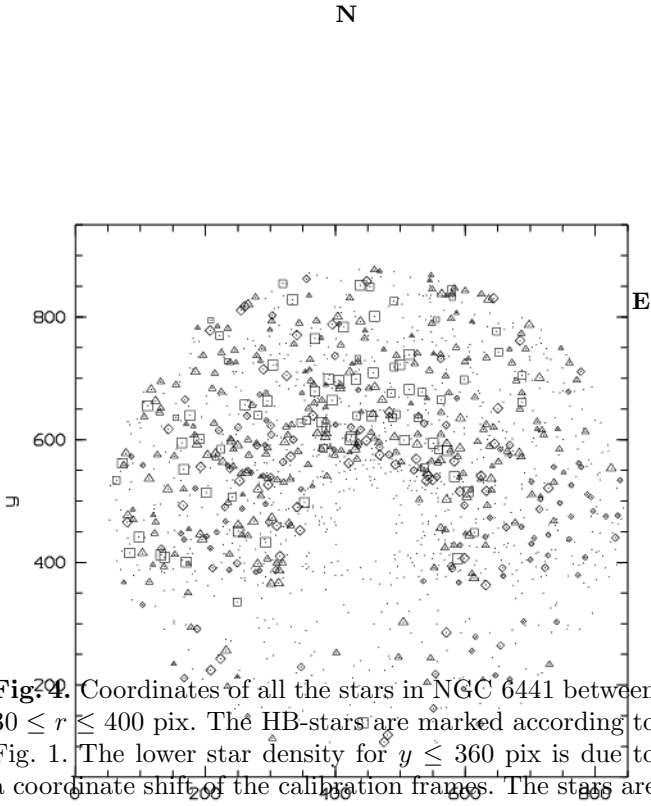


Fig. 4. Coordinates of all the stars in NGC 6441 between $30 \leq r \leq 400$ pix. The HB-stars are marked according to Fig. 1. The lower star density for $y \leq 360$ pix is due to a coordinate shift of the calibration frames. The stars are selected for photometric errors ≤ 0.03 mag. \times

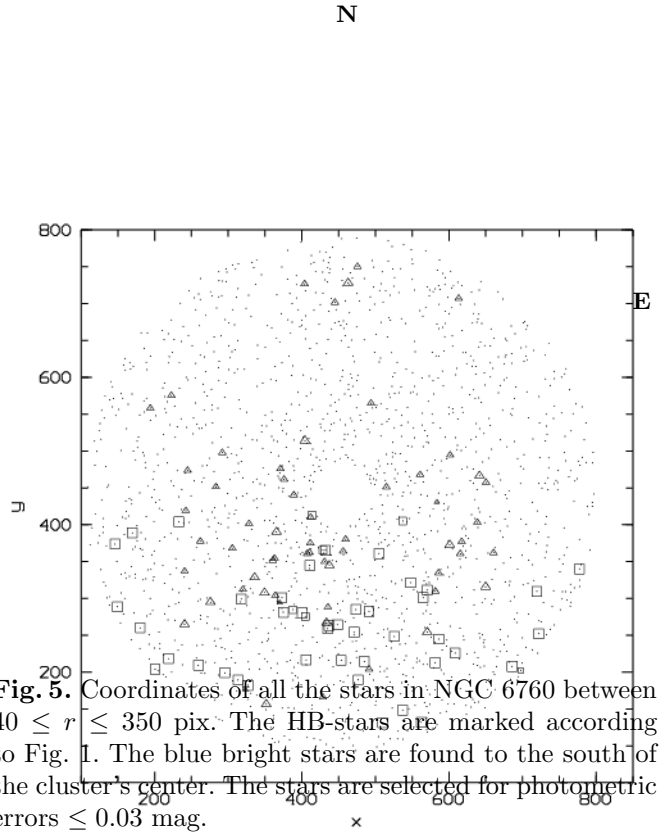


Fig. 5. Coordinates of all the stars in NGC 6760 between $40 \leq r \leq 350$ pix. The HB-stars are marked according to Fig. 1. The blue bright stars are found to the south of the cluster's center. The stars are selected for photometric errors ≤ 0.03 mag. \times

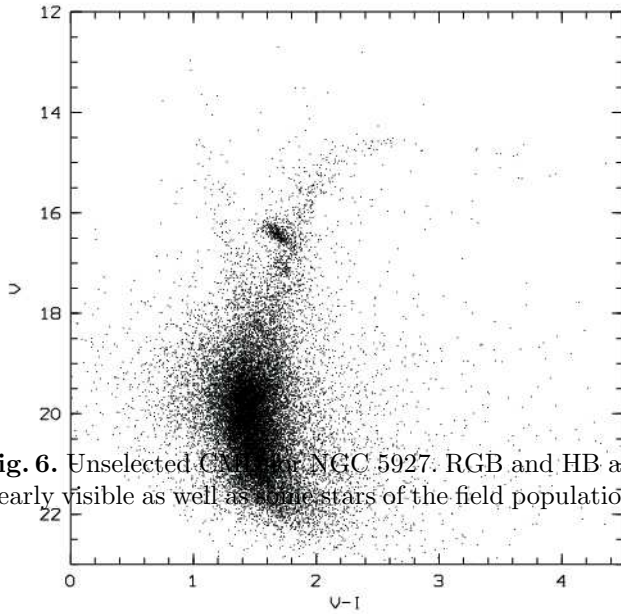


Fig. 6. Unselected CMD for NGC 5927. RGB and HB are clearly visible as well as some stars of the field population.

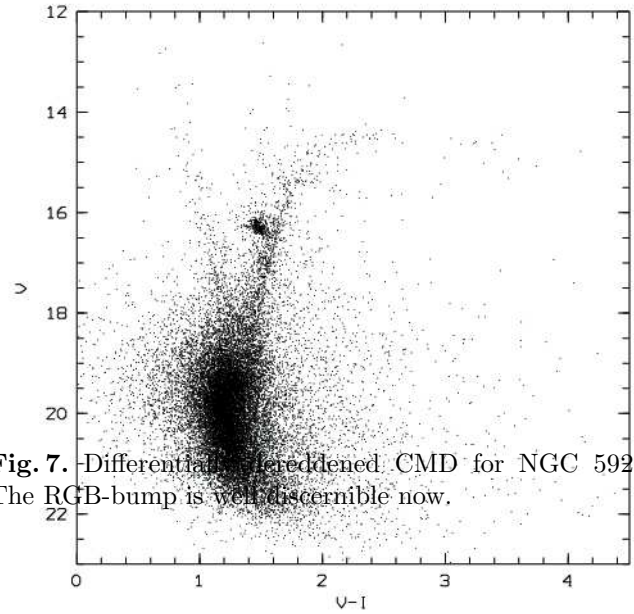


Fig. 7. Differentially dereddened CMD for NGC 5927. The RGB-bump is well discernible now.

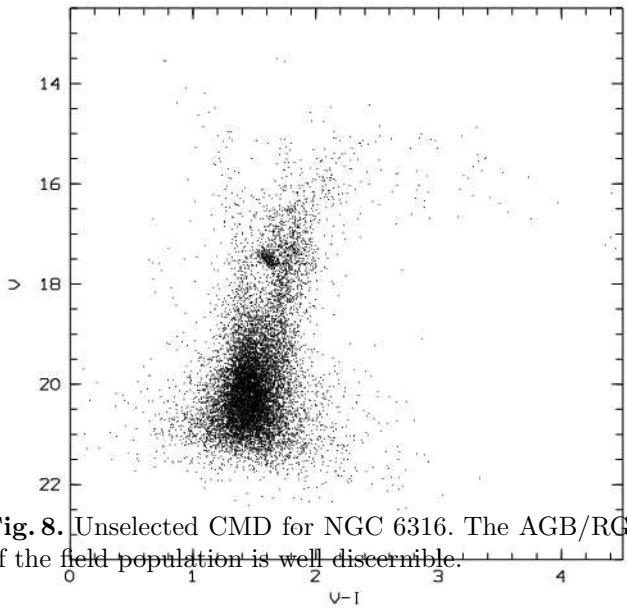


Fig. 8. Unselected CMD for NGC 6316. The AGB/RGB of the field population is well discernible.

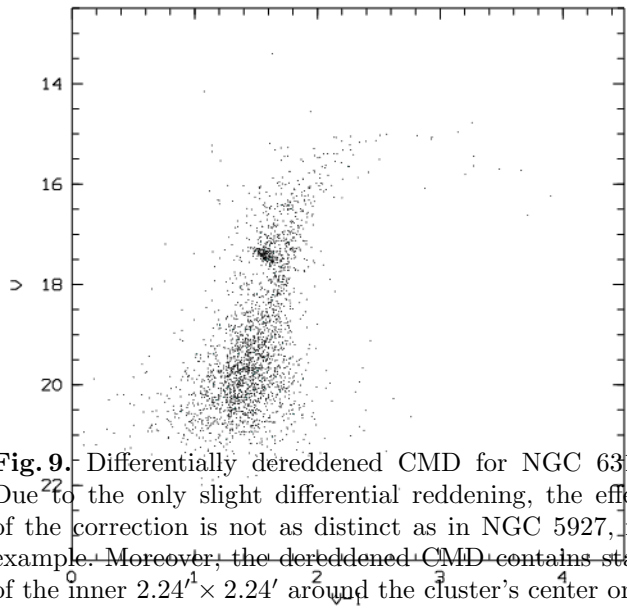


Fig. 9. Differentially dereddened CMD for NGC 6316. Due to the only slight differential reddening, the effect of the correction is not as distinct as in NGC 5927, for example. Moreover, the dereddened CMD contains stars of the inner $2.24' \times 2.24'$ around the cluster's center only (See extinction maps in paragraph 4).

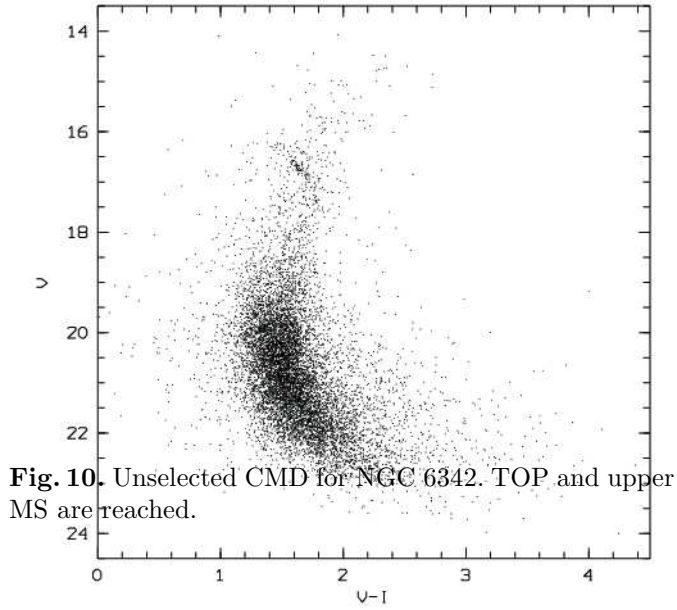


Fig. 10. Unselected CMD for NGC 6342. TOP and upper MS are reached.

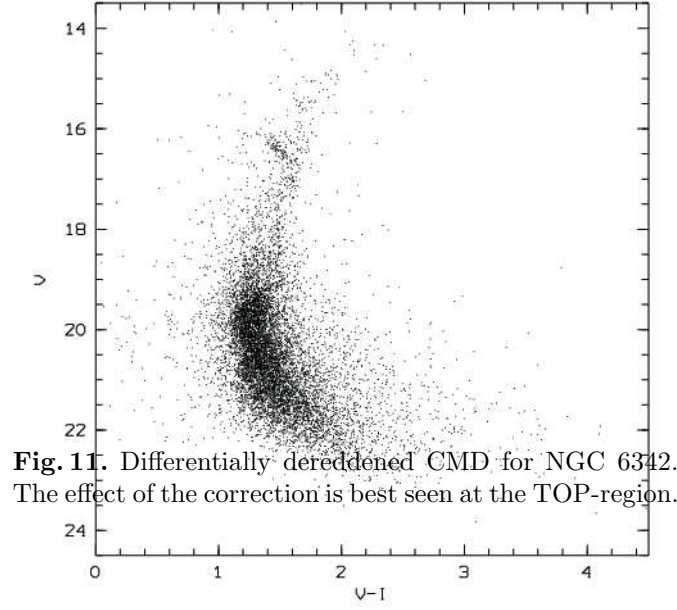


Fig. 11. Differentially dereddened CMD for NGC 6342. The effect of the correction is best seen at the TOP-region.

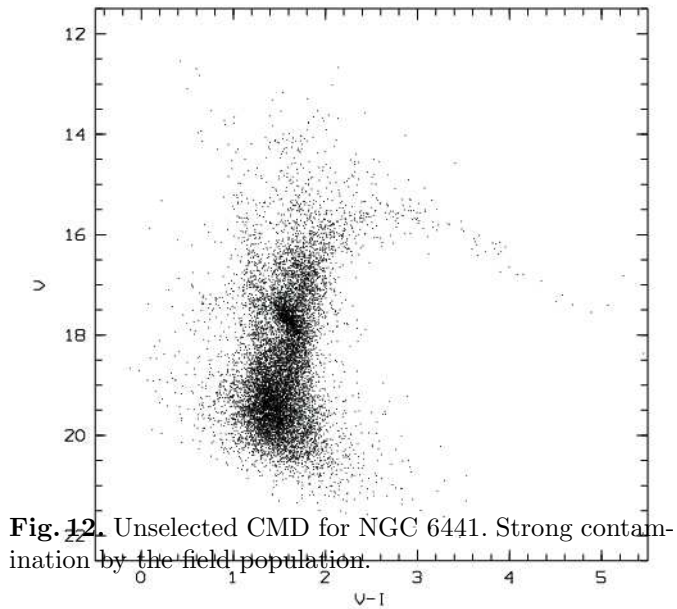


Fig. 12. Unselected CMD for NGC 6441. Strong contamination by the field population.

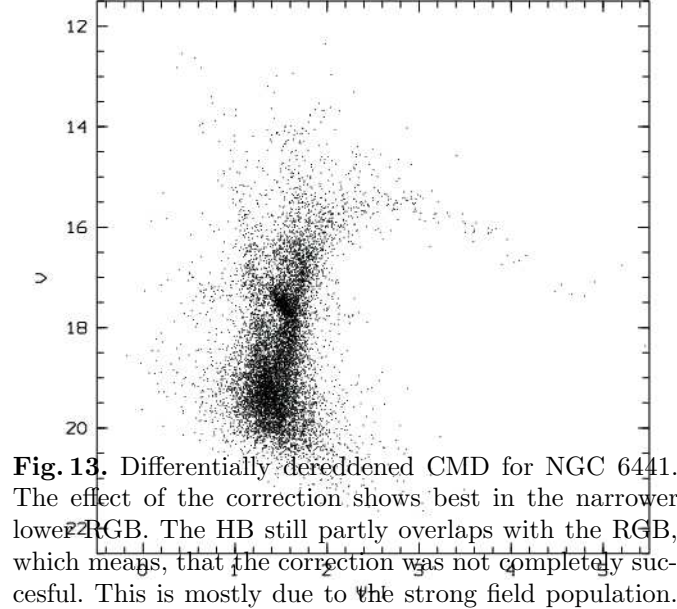


Fig. 13. Differentially dereddened CMD for NGC 6441. The effect of the correction shows best in the narrower lower RGB. The HB still partly overlaps with the RGB, which means, that the correction was not completely successful. This is mostly due to the strong field population.

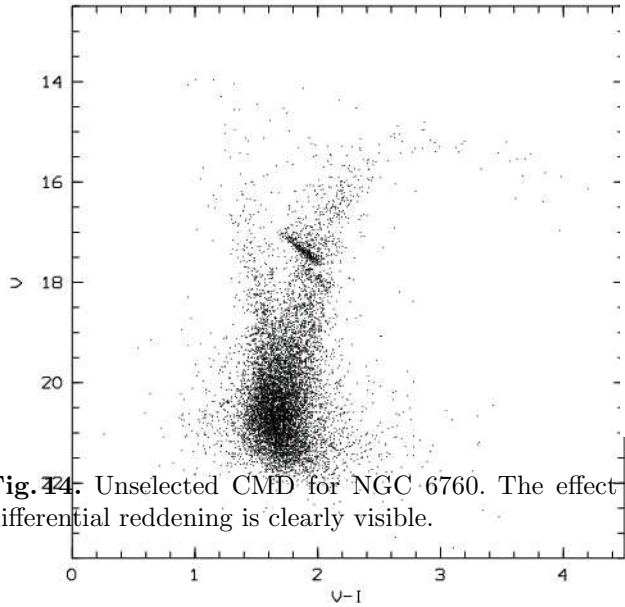


Fig. 14. Unselected CMD for NGC 6760. The effect of differential reddening is clearly visible.

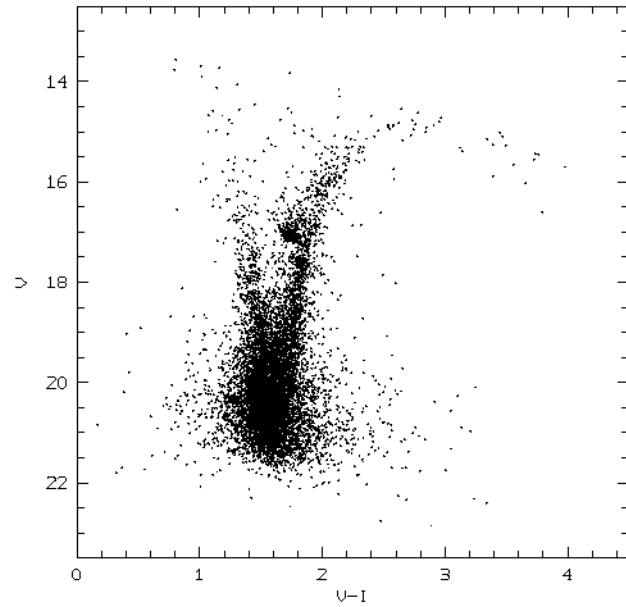


Fig. 15. Differentially dereddened CMD for NGC 6760. The HB lies well to the blue of the RGB, the RGB-bump clearly on the RGB below the HB.

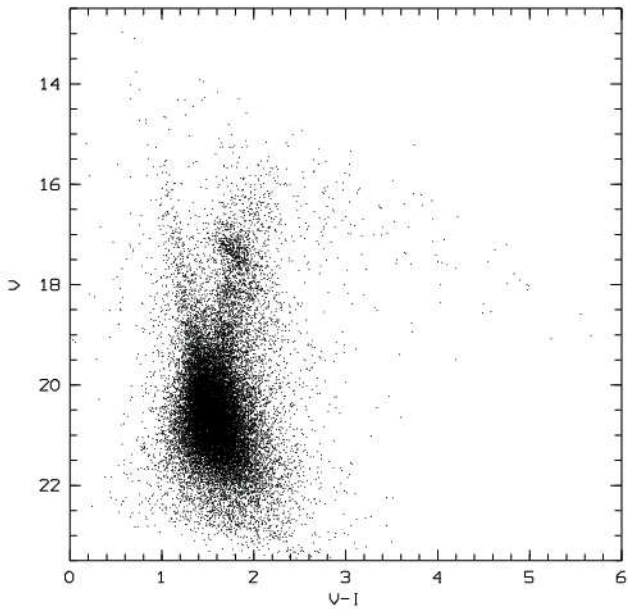


Fig. 16. Unselected CMD for NGC 6528. Below the AGB/RGB there are traces of the background population.

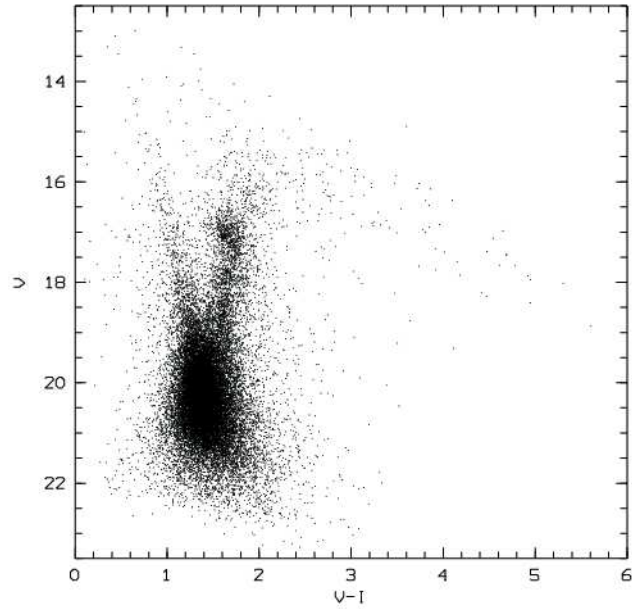


Fig. 17. Differentially dereddened CMD for NGC 6528. The HB still overlaps strongly with the RGB. Thus, the correction was not completely successful due to the strong contamination by field stars. However, the RGB narrowed perceptibly, and the RGB-bump is now visible below the HB.

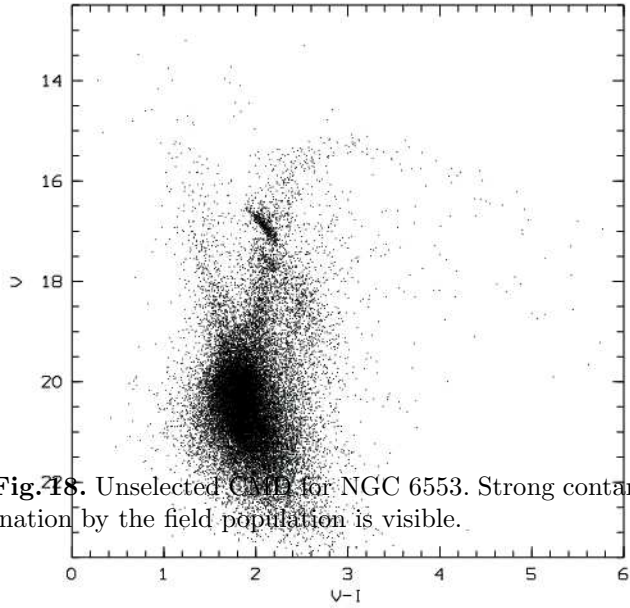


Fig. 18. Unselected CMD for NGC 6553. Strong contamination by the field population is visible.

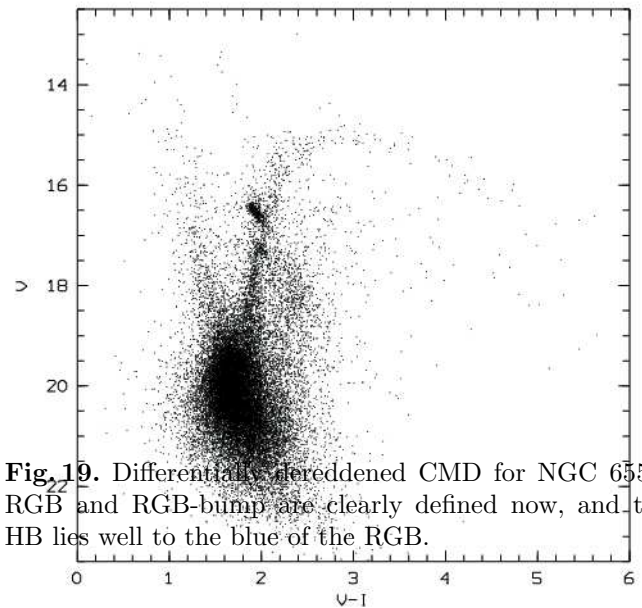


Fig. 19. Differentially dereddened CMD for NGC 6553. RGB and RGB-bump are clearly defined now, and the HB lies well to the blue of the RGB.

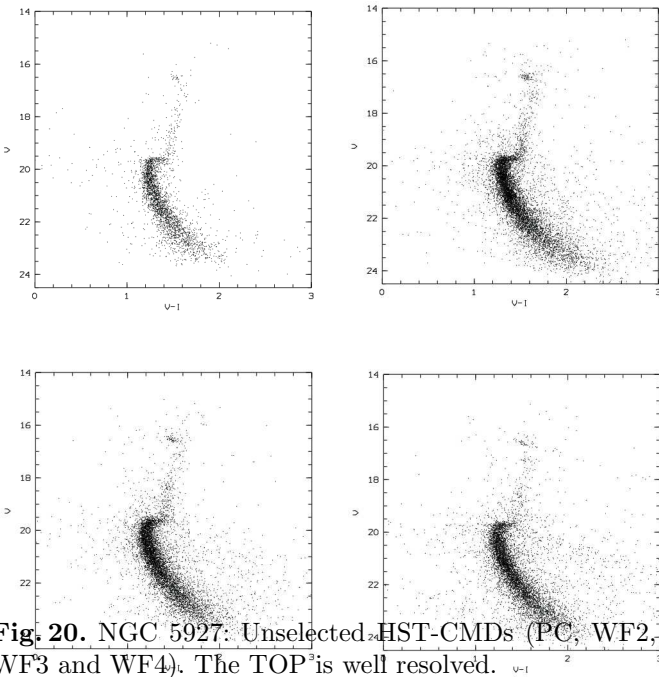


Fig. 20. NGC 5927: Unselected HST-CMDs (PC, WF2, WF3 and WF4). The TOP³ is well resolved.

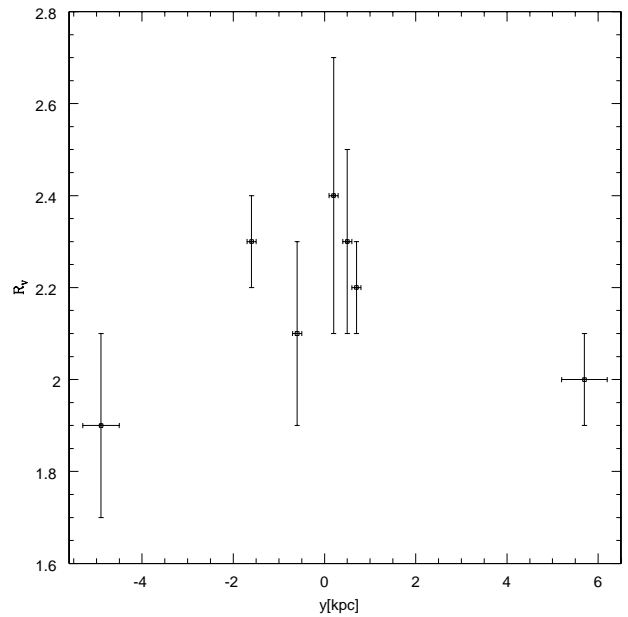


Fig. 21. Slopes of the HBs, i.e. the reddening vectors against galactic longitude (here in cartesian coordinates).

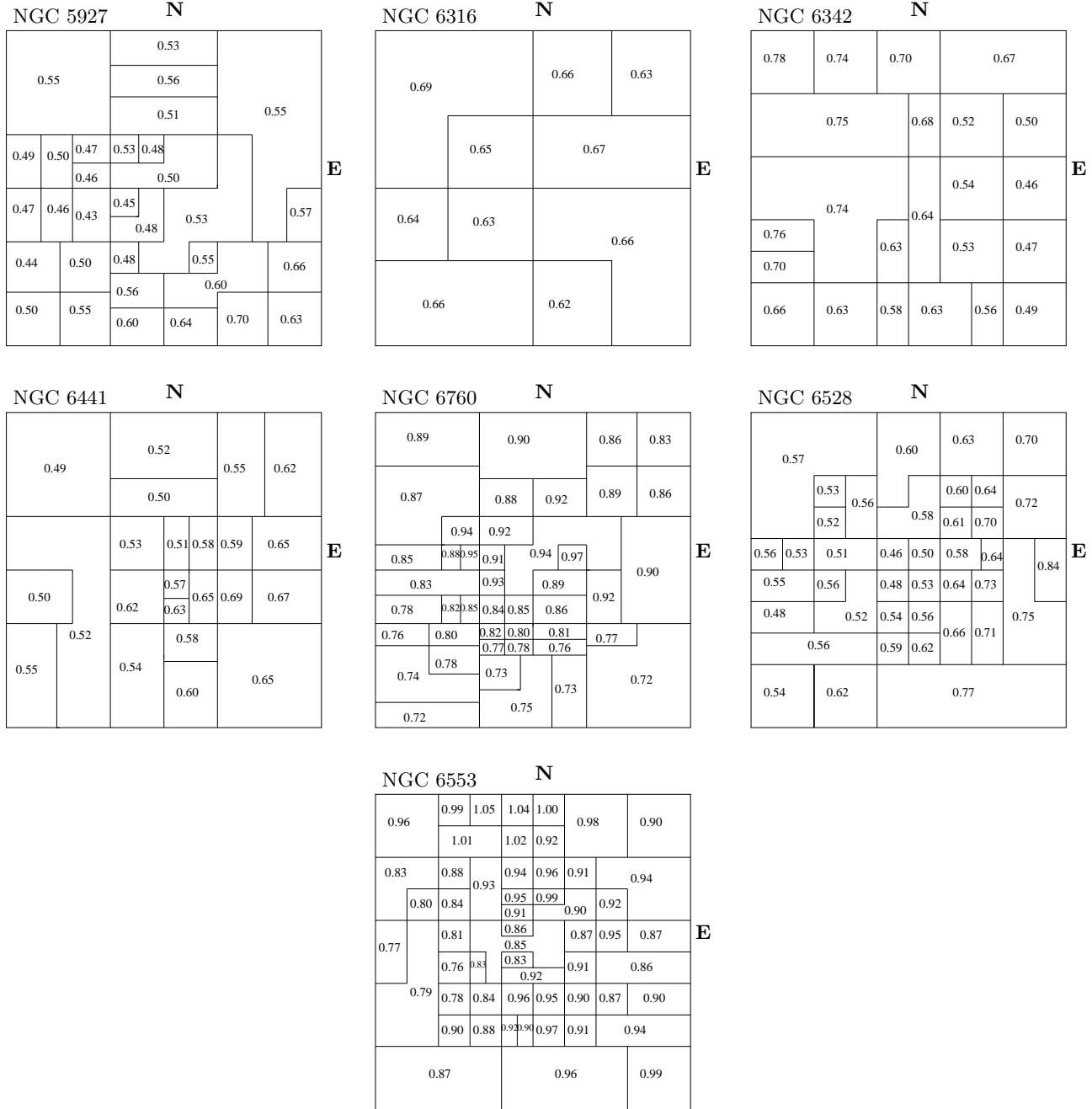


Fig. 22. Extinction maps for NGC 5927 to NGC 6553, derived from plotting CMDs for each of the areas. The numbers in the subfields give the absolute reddening derived via isochrone fitting. The differential reddening was determined using the minimal absolute reddening as a point of reference. As the derived scale of reddening variation strongly depends on the number of stars, the resulting scales can only be estimates for upper boundaries. The maps cover $5.7' \times 5.7'$, i.e. they cover the whole area of the original frames. An exception is made with NGC 6136, where we constrained the map to the inner $2.24' \times 2.24'$, because of the clusters small size.

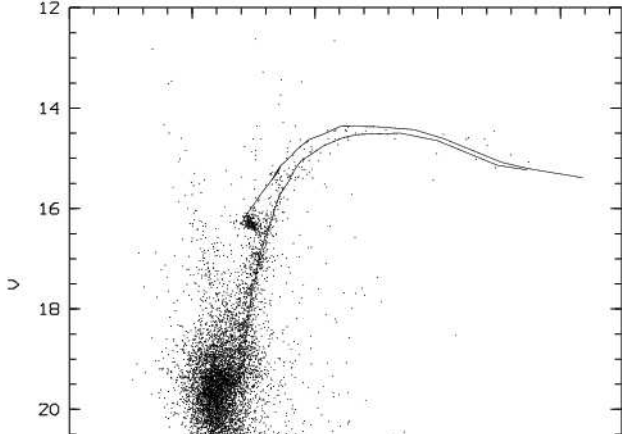


Fig. 23. Isochrone fitting for NGC 5927. $[M/H] = -0.40$ dex, $t = 14.5$ kyr. The CMD is selected for photometric errors ≤ 0.04 mag and for radii ($50 \leq r \leq 400$) pix. The first selection gives preference to brighter stars, i.e. to stars which not necessarily are cluster members. This effect is counterbalanced by the second selection.

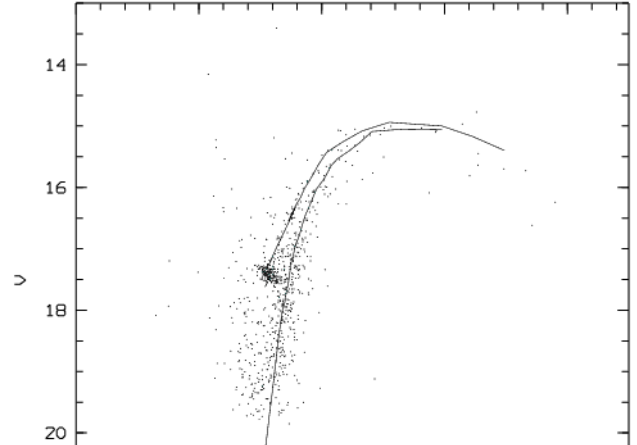


Fig. 24. NGC 6316, selected for photometric errors ≤ 0.04 mag and with an isochrone $[M/H] = -0.70$, $t = 14.5$ kyr. The radial selection is due to the correction for differential reddening (see Figs. 9 and 22).

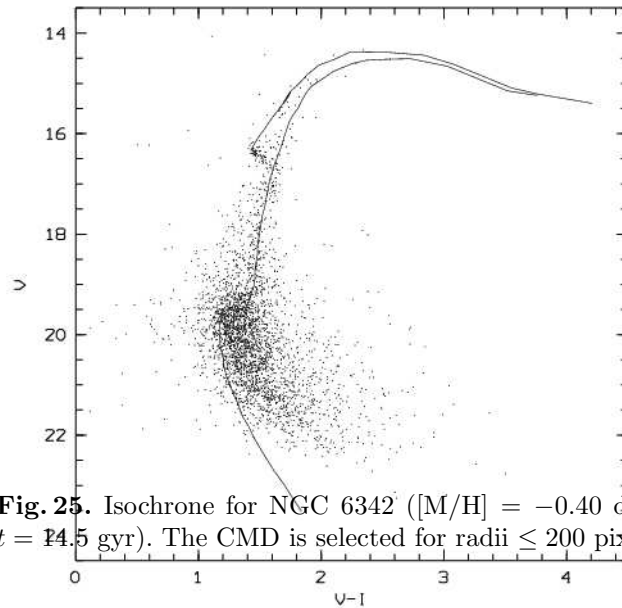


Fig. 25. Isochrone for NGC 6342 ($[M/H] = -0.40$ dex, $t = 14.5$ kyr). The CMD is selected for radii ≤ 200 pix.

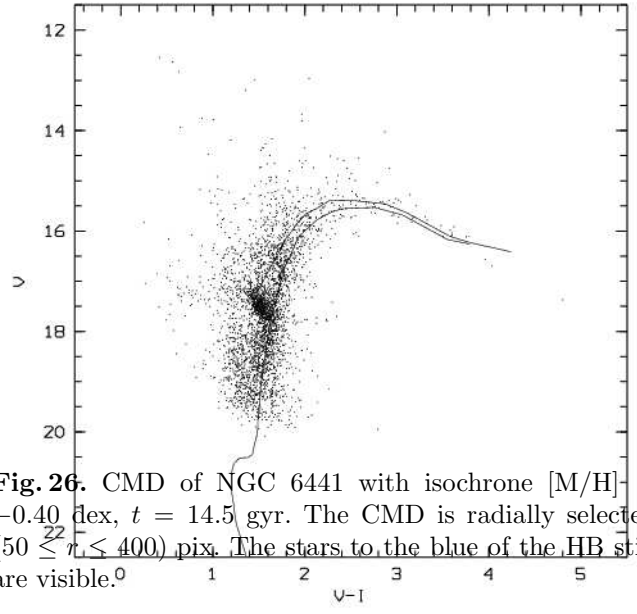


Fig. 26. CMD of NGC 6441 with isochrone $[M/H] = -0.40$ dex, $t = 14.5$ kyr. The CMD is radially selected ($50 \leq r \leq 400$) pix. The stars to the blue of the HB still are visible.

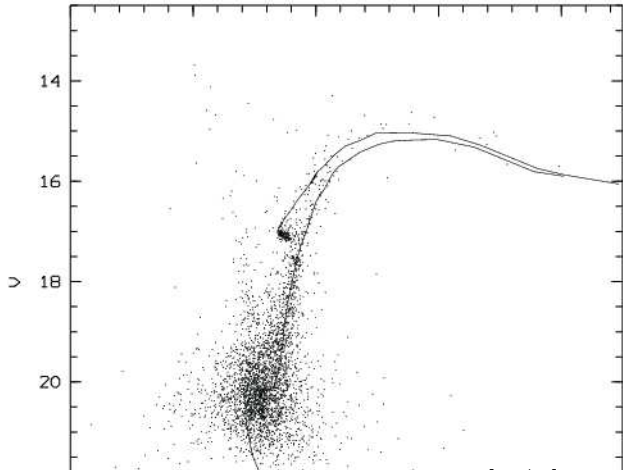


Fig. 27. The isochrone for NGC 6760 with $[M/H] = -0.40$ dex and $t = 14.5$ gyr is slightly too metal-rich, as the AGB/RGB arcs above the model. This result is corroborated by the metallicity-estimates given below. The CMD is radially selected for $100 \leq r \leq 300$ pix.

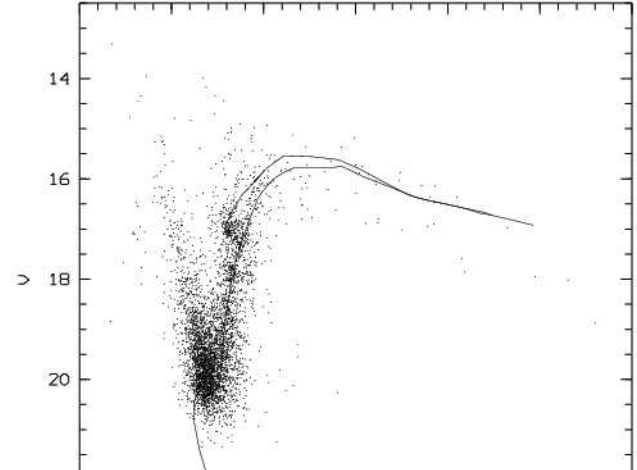


Fig. 28. The radially selected CMD of NGC 6528 clearly shows the two AGB/RGB's of the cluster's and the background population. The isochrone ($[M/H] = 0.0$ dex, $t = 14.5$ gyr) is slightly too metal-rich as well.

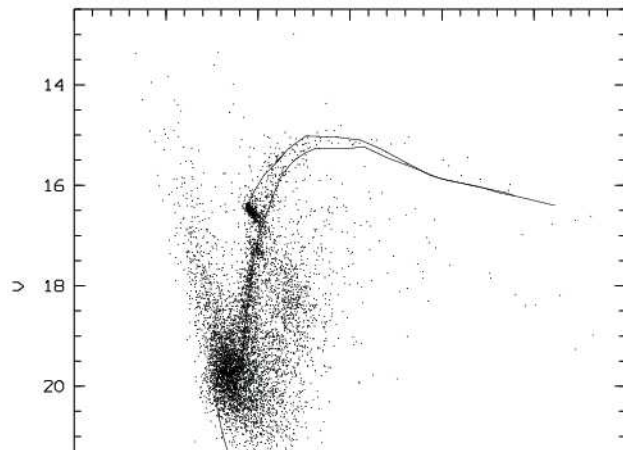


Fig. 29. Radially selected CMD ($50 \leq r \leq 400$ pix) of NGC 6553 with an isochrone of $[M/H] = 0.0$ dex and $t = 14.5$ gyr. The strongly differentially reddened field population is now clearly separated from the cluster (to the red of the lower RGB). The CMD is also selected for photometrical errors ≤ 0.05 mag.

5. The Globular Cluster Parameters

This section deals with the determination of the metallicity, reddening and distance using the *differentially dereddened* CMDs. There are two possible ways to achieve the goal. In the first, theoretical models are compared with the CMDs, in the second, empirical relations between parameters and loci in the CMDs are used.

5.1. Isochrone fitting

To derive metallicity, distance and absolute reddening via isochrone fitting, we used the Padova-tracks (Bertelli et al. 1994) with a fixed age of 14.5 Gyr ($\log(\text{age}) = 10.160$). Isochrones with different ages ($10.120 \leq \log(\text{age}) \leq 10.200$) led to identical results. To avoid systematic errors, we used the middle of the broadened structures to fit the isochrones by eye. These loci are easily determined for the ascending part of the RGB, as it runs more or less perpendicular to the reddening vector. Regarding the upper part of the RGB, we take into account that we cannot distinguish between the AGB and the RGB in our diagrams. Hence, the densest regions of the AGB/RGB lie between the model's tracks. We additionally used the HB and the lower part of the RGB, as far as they were accessible. The parameters resulting from the isochrone fit are given in Table 2.

NGC	$(m - M)_V$	E_{V-I}	[M/H]
5927	15.45 ± 0.03	0.43 ± 0.02	-0.40
6316	16.76 ± 0.04	0.62 ± 0.03	-0.70
6342	15.36 ± 0.04	0.46 ± 0.03	-0.40
6441	16.48 ± 0.05	0.49 ± 0.03	-0.40
6760	16.18 ± 0.04	0.72 ± 0.03	-0.40
6528	15.94 ± 0.05	0.46 ± 0.03	0.00
6553	15.42 ± 0.04	0.76 ± 0.03	0.00

Table 2. Distance modulus $(m - M)_V$, total reddening E_{V-I} and metallicity [M/H] of all the sample's clusters derived by isochrone fitting. The errors are eye-estimates of how accurately we could place the isochrones. Note that the isochrones are fitted to the differentially dereddened CMDs.

Figures 23 to 29 show the differentially dereddened CMDs with the fitted isochrones. For a discussion and comparison of these parameters with the literature, see paragraph 5.3.

5.2. Metallicity and reddening: relations

5.2.1. Metallicity

The luminosity difference between HB and the turn over of the AGB/RGB in $(V, V - I)$ -CMDs is very sensitive to metallicity in the metal-rich domain (e.g. Ortolani et al.

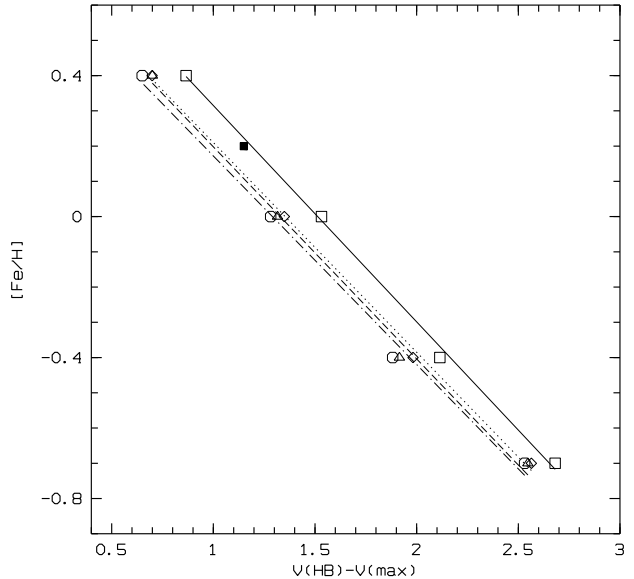


Fig. 30. [M/H] – ΔV -relation for different ages. The open symbols stand for the isochrone-values. Squares, lines: 9.8 Gyr, diamonds, dotted: 13.2 Gyr, triangles, dashed: 14.5 Gyr, circles, dash-dotted: 15.8 Gyr. The filled square represents the value for NGC 6791 (Garnavich et al. 1994).

1997). Moreover, it is a differential metallicity indicator, thus it is independent of absolute colour or luminosity, in contrast to the [M/H] – $(V - I)_{0,g}$ -method (see e.g. Sarajedini 1994). We present a preliminary linear calibration of this method,

$$[\text{M}/\text{H}] = a(V_{\text{HB}} - V_{\text{RGB}}^{\text{max}}) + b, \quad (3)$$

as there has not been any so far. Because there still are only very few $(V, V - I)$ -CMDs which clearly show both the HB and turn over of the AGB/RGB and which have reliable metallicity determinations, we used the Padova-isochrones and a CMD of NGC 6791 (Garnavich et al. 1994) to set up a calibration. NGC 6791 is one of the richest old open clusters with a good metallicity determination and it is therefore suitable to serve as a zero-point check.

As the form of the RGB depends slightly on age as well (e.g. Stetson et al. 1996), we have to check this dependence before applying our calibration. Fig. 30 shows the linear relation between [M/H] and $\Delta V \equiv V_{\text{HB}} - V_{\text{max}}$ for four GC-ages. Table 3 contains the respective coefficients. As the metal-poorest isochrones of the Padova-sample ([M/H] = -1.70, 1.30 dex) do not show a maximum of the AGB/RGB, they have not been used. Fig. 30 makes clear that the age has only a minor influence on the resulting metallicity. To be consistent with the isochrone-fit, we used the relation for $\log(\text{age}) = 10.160$.

NGC	V_{HB}	V_{RGB}^{max}	ΔV	$[M/H]$ [dex]	$[M/H]_1$	$[M/H]_2$
5927	16.30 ± 0.03	14.49 ± 0.04	1.81	-0.29 ± 0.08	-0.37	-1.08
6316	17.42 ± 0.05	15.09 ± 0.04	2.33	-0.60 ± 0.09	-0.55	
6342	16.47 ± 0.05	14.44 ± 0.06	2.03	-0.42 ± 0.09	-0.65	
6441	17.51 ± 0.07	15.53 ± 0.07	1.98	-0.39 ± 0.10	-0.53	
6760	17.08 ± 0.02	14.81 ± 0.04	2.27	-0.57 ± 0.09	-0.52	
6528	17.07 ± 0.06	15.74 ± 0.08	1.33	0.00 ± 0.09	-0.17	-0.15
6553	16.52 ± 0.07	15.13 ± 0.06	1.39	-0.04 ± 0.08	-0.25	-0.10

Table 4. Metallicities of all GCs via the differentially dereddened CMDs. Column $[M/H]$ contains the values derived by the $[M/H] - \Delta V$ -relation. The values of column $[M/H]_1$ have been taken from Harris (1996). Column $[M/H]_2$ gives additional values as discussed in the text. The errors only take account of the uncertainties of the luminosities and the calibration errors of Table 3.

$\log(age)$	a [dex/mag]	b [dex]
9.990	-0.614 ± 0.020	0.929 ± 0.026
10.120	-0.595 ± 0.017	0.805 ± 0.024
10.160	-0.602 ± 0.032	0.800 ± 0.043
10.200	-0.592 ± 0.033	0.764 ± 0.045

Table 3. Calibration coefficients of the $[M/H] - \Delta V$ -relation for different cluster ages. The calibration equation is $[M/H] = a\Delta V + b$.

To estimate the metallicities of our clusters, we now only have to measure the relevant luminosities. The results are given in Table 4. The value for NGC 5927 given in column $[M/H]_2$ relates to a single star (François 1991); NGC 6528 and NGC 6553 are from Richtler et al. (1998) and Sagar et al. (1998).

5.2.2. Reddening

It should be remembered, that we used the differentially dereddened CMDs to determine the parameters. Thus, the given reddenings are minimal ones.

As mentioned above, the absolute colour of the RGB at the level of the HB can be used to estimate the metallicity. Conversely (Armandroff 1988), if we know the metallicity, we can determine the absolute colour $(V - I)_{0,g}$ and thus the absolute reddening of the cluster.

These relations between colour $(V - I)_{0,g}$ and metallicity are well calibrated for the metal-poor to intermediate regime. However, it is difficult to set up a calibration for the metal-rich regime of our clusters. Linear calibrations have been provided by e.g. Sarajedini (1994). A more recent calibration by Caretta & Bragaglia (1998a) uses a 2nd order polynomial. To set up a calibration for the metal-rich regime we used again the Padova-tracks together with NGC 6791 to derive the coefficients for a relation of the form

$$(V - I)_{0,g} = a + b \cdot [M/H] + c \cdot [M/H]^2 + d \cdot [M/H]^3 \quad (4)$$

In addition, we used the $[M/H]$ and $(V - I)_{0,g}$ values for M67 given by Montgomery et al. (1993) to check the zero

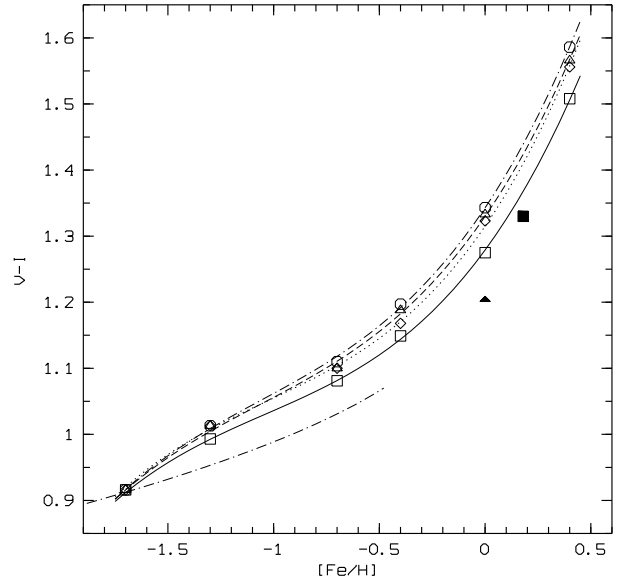


Fig. 31. Calibration of the non-linear $(V - I)_{0,g} - [M/H]$ -relation for different ages. The key for the symbols is the same as used in Fig. 30, except for the filled triangle denoting the $(V - I)_{0,g} - [M/H]$ pair of M67. In addition, the quadratic relation of Caretta & Bragaglia (1998a) is plotted in dash-dotted line. It intersects our relation at low $[Fe/H]$ but shows a difference of $\Delta(V - I) = 0.4$ mag in the more metal-rich regime.

point. Taking into account that M67 is even younger than NGC 6791 by 3 to 5 Gyrs, the measured quantities fit reasonably well. Table 5 contains the calibration coefficients, Fig. 31 the graphic relations, again for different ages. As above, we used the relation for $\log(age) = 10.160$.

Using the metallicities listed in Table 4, column $[M/H]$, we get the absolute reddening as given in Table 6. Metallicities as well as reddenings fit very well with the values derived via isochrone-fitting, but are significantly lower than the values given in the literature. This is partly explained by the fact that we take the minimal reddening

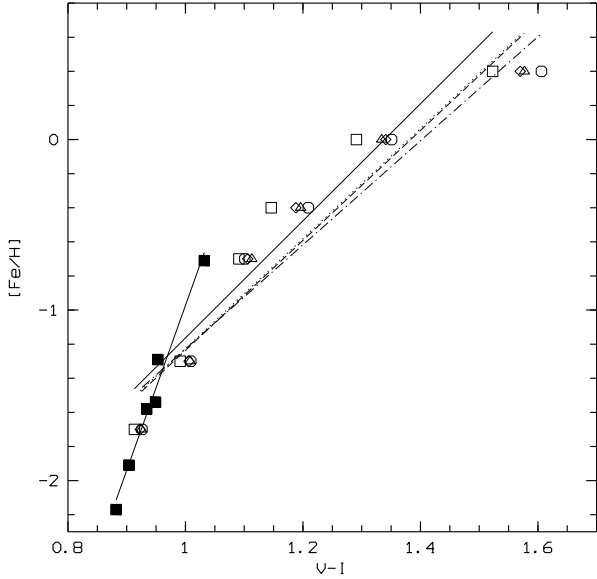


Fig. 32. Calibration of the linear $[M/H] - (V - I)_{0,g}$ -relation according to Sarajedini (filled symbols) in comparison to the recalibration for higher metallicities. The key for the symbols is the same as used in Fig. 30, except for the filled symbols.

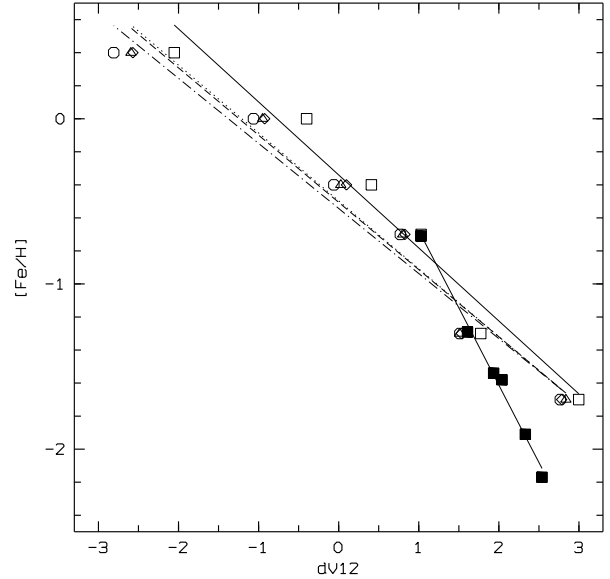


Fig. 33. Calibration of the linear $[M/H] - \Delta V_{1,2}$ -relation according to Sarajedini (filled symbols) in comparison to the recalibration for higher metallicities. The key for the symbols is the same as used in Fig. 30, except for the filled symbols.

from the reddening map. Another part of the explanation may be that previous isochrone fits tend to use the red ridge of the RGB and thus overestimate the reddening.

Sarajedini (1994) proposed a method to simultaneously determine metallicity and reddening. For this, he used the (linear) $[M/H] - (V - I)_{0,g}$ -relation and the dependence of metallicity on the luminosity of the RGB at the absolute colour of $V - I = 1.2$ mag, in linear form as well. He calibrated both relations for a metallicity range of $(-2.2 \leq [M/H] \leq -0.70)$ dex. We recalibrated these relations in order to use them for our clusters. Using NGC 6791 and the Padova-tracks. The graphic results are shown in Figs. 32 and 33; the calibration coefficients are given in Table 7. For a discussion and new calibration of Sarajedini's method see Caretta & Bragaglia (1998a). We did not make use of this method, as the extrapolation of Sarajedini's calibration did not seem to be advisable, with reference to Figs. 32 and 33.

5.2.3. Distance

The brightness M_V^{HB} of the horizontal branch is the best distance indicator for GCs. However, there is a lively discussion on how this brightness depends on the metallicity of the cluster.

We take the LMC distance as the fundamental distance for calibrating the zero point in the relation between metallicity and horizontal branch/RR Lyrae bright-

ness. The third fundamental distance determination beside trigonometric parallaxes and stellar stream parallaxes is the method of Baade-Wesselink parallaxes. It had been applied to the LMC in its modified form known as Barnes-Evans parallaxes. So far, it has been applied to Cepheids in NGC 1866 (Gieren et al. 1994), and the most accurate LMC distance until now stems from the period-luminosity relation of LMC Cepheids by Gieren et al. (1998). We adopt the distance modulus from the latter work, which is 18.46 ± 0.06 mag, and which is in very good agreement with most other work (e.g. Tanvir 1996).

If we adopt the apparent magnitude of RR Lyrae stars in the LMC from Walker (1992), 18.94 ± 0.1 mag for a metallicity of $[Fe/H] = -1.9$ dex, and the metallicity dependence from Caretta et al. (1998b), one gets

$$M_V(RR) = (0.18 \pm 0.09)([Fe/H] + 1.6) + 0.53 \pm 0.12 \quad (5)$$

This zero-point is in excellent agreement with the one derived from HB-brightnesses of old LMC globular clusters, if the above metallicity dependence is used (Olszewski et al. 1991).

With relation 5, with the reddenings (as shown in Table 6, column E_{V-I}^{rel}) and with the extinction $A_V = R_V^I E_{V-I}$ we can calculate the distance moduli

$$(m - M)_0 = V_{HB} - A_V - M_V^{HB} \quad (6)$$

The values for M_V^{HB} and $[M/H]$ are listed in Table 4, and the results are given in Table 8. R_V^I comes from Table 1.

5.3. Comparison

The distances determined via the $M_{HB} - [M/H]$ -relation are larger than those determined by the isochrone-fitting (Table 9). However, as the related reddenings do not show any significant differences, this effect is attributed to the $M_{HB} - [M/H]$ -relation and the isochrone-fitting itself. As described above, the isochrone fitting is lacking the desired accuracy especially because the TOP cannot be resolved for most of the clusters. Moreover, the fact that AGB and RGB cannot be distinguished in our CMDs leads to a systematic error in the isochrone distances in the sense that the isochrones tend to have been fitted with brightnesses which are too large. In the following, we discuss some possible explanations for differences between distances taken from the literature and this work. It should be remembered that the distance errors amount to about 10%.

1. The distance to NGC 6528 increases by nearly 30% compared to Richtler et al. (1998). Taking into account, that the isochrone (Fig.28) might have been fitted slightly too low, we still get a distance of about 8.1 kpc. Moreover, Richtler et al. determine the absolute reddening via the differentially reddened CMD, which leads to larger values ($0.6 \leq E_{V-I} \leq 0.8$) compared to our $E_{V-I} = 0.46$. Thus the distance modulus decreases by about 0.4 mag, as equation 6 is corrected more strongly on reddening. Finally, the different slopes of the reddening vector have to be regarded. Richtler et al. assume $A_V/E_{V-I} = 2.6$, our slope, which we determined via the slope of the HB, amounts to $A_V/E_{V-I} = 2.4$. On the whole, we get a difference between Richtler et al. and this work of 0.7 mag in the distance modulus.
2. In the CMDs of NGC 5927 and 6760 the differential reddening becomes noticeable especially along the steep part of the RGB, as this is running nearly perpendicularly to the reddening vector. Around the turn over of the AGB/RGB and for its redder part, it leads to an elongation, but not to a broadening of the structures. Fitting an isochrone to the broadened RGB, one generally would use the middle of the RGB as an orientation, as one cannot distinguish between reddening effects and photometric errors in the outer regions. However, the red part of the AGB/RGB approximately keeps its unextinguished brightness. Thus the differential reddening might be overestimated, which leads to decreasing distances. A similar point can be made for the determination of E_{V-I} via the $(V-I)_{0,g} - [M/H]$ -relation. Measuring the colour $(V-I)_g$ in the differentially reddened diagram is best done at the middle of the broadened RGB again. This leads to an increased reddening, i.e. the distance modulus will be corrected too strongly for extinction. Overestimating the colour by 0.1 mag leads to a decrease in distance of about 10%.

3. For NGC 6441, Harris (1996) cites a value of $V_{HB} = 17.10$ mag. From our CMD we get 17.66 mag. This lower brightness is supported by (V,B-V)-CMDs of Rich et al. (1997), especially as Harris' value comes from a CMD by Hesser & Hartwick (1976), whose lower limiting brightness is around 17.3 mag.
4. The distances as determined via the $[M/H] - \Delta V$ - and the $(V-I)_{0,g} - [M/H]$ -relation relate to the differentially dereddened CMDs, i.e to the minimal absolute reddening. However, the papers we obtained the cited values from (Table 6), do not take differential reddening into account (e.g. Armandroff (1988) for NGC 6342 and 6760, Ortolani et al. (1990, 1992) for NGC 6528 and 6553). So their absolute reddenings are systematically larger and the distances smaller. Interestingly, the absolute reddening for NGC 6316 of $E_{V-I} = 0.63$ mag as determined in this work fits very well the value of $E_{V-I} = 0.61$ mag given by Davidge et al. (1992); NGC 6316 shows the smallest differential reddening ($\delta E_{V-I} = 0.07$ mag) of our cluster sample.
5. Finally, the distances depend on the assumed extinction law. The value varies between $3.1 \leq R_V^B \leq 3.6$ (Savage & Mathis 1979, Grebel & Roberts 1995, see Fig 21 and discussion). This effect should have the strongest influence on the distances as determined in this work. Taking an absolute reddening of 0.5 mag, the variation between the above cited values results in a difference of 0.25 mag in the distance modulus. This corresponds to about 25% of the distance in kpc.

The distance error mostly depends on the absolute reddening used. The errors in the metallicities have only a minor influence on the distances (see Table 5). They amount to around 3% of the total distance in kpc. In conclusion, the increased distances r_{rel} (Table 9) are due to the fact that we determine the distance-relevant parameters using the differentially dereddened CMDs.

NGC	r_{Harris}	r_{iso}	r_{rel}	r_{lit}
5927	7.4	8.4	8.9	
6316	11.5	12.3	12.0	
6342	9.1	7.4	8.7	
6441	9.7	11.8	13.9	
6760	7.3	8.9	9.5	
6528	7.4	9.3	10.7	6.6
6553	4.7	5.4	6.2	5.2

Table 9. Comparison of the distances taken from Harris (1996), r_{Harris} , with the values of this work. r_{iso} and r_{rel} contain the distances determined via isochrone-fitting and $M_{HB} - [M/H]$ -relation. The last column shows recently determined distances for NGC 6528 (Richtler et al. 1998) and for NGC 6553 (Guarnieri et al. 1998).

$\log(age)$	a	b	c	d
9.990	1.279 ± 0.002	0.438 ± 0.004	0.287 ± 0.010	0.092 ± 0.005
10.120	1.315 ± 0.003	0.468 ± 0.007	0.307 ± 0.016	0.099 ± 0.008
10.160	1.330 ± 0.004	0.467 ± 0.008	0.281 ± 0.021	0.088 ± 0.011
10.200	1.343 ± 0.006	0.479 ± 0.006	0.289 ± 0.014	0.091 ± 0.008

Table 5. Calibration coefficients for the $(V - I)_{0,g} - [M/H]$ -relation (equation 4).

NGC	E_{V-I}^{iso}	$(V - I)_{HB}$	$(V - I)_{0,g}$	E_{V-I}^{rel}	E_{V-I}^{lit}	literature
5927	0.43 ± 0.02	1.63 ± 0.02	1.22 ± 0.04	0.41 ± 0.05	0.66	Sarajedini & Norris (1994)
6316	0.62 ± 0.03	1.76 ± 0.03	1.13 ± 0.06	0.63 ± 0.06	0.61	Davidge et al. (1992)
6342	0.46 ± 0.03	1.65 ± 0.04	1.18 ± 0.05	0.47 ± 0.06	0.65	Armandroff & Zinn (1998)
6441	0.49 ± 0.03	1.64 ± 0.04	1.19 ± 0.05	0.46 ± 0.06	0.64	Deutsch et al. (1996)
6760	0.72 ± 0.03	1.88 ± 0.02	1.14 ± 0.05	0.74 ± 0.06	1.07	Armandroff & Zinn (1998)
6528	0.46 ± 0.03	1.79 ± 0.04	1.33 ± 0.06	0.46 ± 0.06	0.70	Richtler et al. (1998)
6553	0.76 ± 0.03	2.08 ± 0.04	1.31 ± 0.06	0.77 ± 0.06	0.95	Sagar et al. (1998)

Table 6. Absolute reddening for all GCs. Column E_{V-I}^{iso} contains values derived via isochrone-fitting, column E_{V-I}^{rel} values via $(V - I)_{0,g} - [M/H]$ -relation. $(V - I)_g$ gives the colour of the RGB at the level of V_{HB} , $(V - I)_{0,g}$ the corresponding dereddened colour, calculated via the $(V - I)_{0,g} - [M/H]$ -relation. In the last column, we cited values from literature and their sources, which, of course, cannot be more than a selection. Any measurement of colours was done in the differentially dereddened CMDs, which provides the explanation for the difference between our values and that taken from other works.

	a_{V-I}	b_{V-I}	$a_{1,2}$	$b_{1,2}$
Padova 7.9 Gyr	3.432	-4.595	-0.442	-0.340
Padova 13.2 Gyr	3.225	-4.451	-0.441	-0.497
Padova 14.5 Gyr	3.222	-4.458	-0.407	-0.506
Padova 15.8 Gyr	3.052	-4.280	-0.394	-0.543
Sarajedini	9.668	10.64	-0.9367	0.2606

Table 7. Coefficients for Sarajedini- and Padova-relations. The equations have the form $[M/H] = a_{V-I}(V - I)_{0,g} + b_{V-I}$ and $[M/H] = a_{1,2}\Delta V_{1,2} + b_{1,2}$. The errors are $\Delta a_{V-I} = 0.43$, $\Delta b_{V-I} = 0.23$, $\Delta a_{1,2} = 0.04$ und $\Delta b_{1,2} = 0.16$.

NGC	A_V	M_V^{HB}	$(m - M)_0$	r	r_{Harris}
5927	0.79 ± 0.12	0.77 ± 0.12	14.75 ± 0.17	8.9 ± 0.7	7.4
6316	1.32 ± 0.18	0.71 ± 0.13	15.39 ± 0.23	12.0 ± 1.2	11.5
6342	1.04 ± 0.15	0.74 ± 0.13	14.69 ± 0.20	8.7 ± 0.8	9.1
6441	1.05 ± 0.16	0.75 ± 0.13	15.70 ± 0.21	13.8 ± 1.3	9.7
6760	1.48 ± 0.13	0.72 ± 0.13	14.88 ± 0.19	9.5 ± 0.8	7.3
6528	1.11 ± 0.16	0.82 ± 0.12	15.15 ± 0.24	10.7 ± 1.1	7.4
6553	1.76 ± 0.13	0.81 ± 0.12	13.95 ± 0.24	6.2 ± 0.7	4.7

Table 8. Distances of GCs via $M_V^{HB} - [M/H]$ -relation. The given errors only account for the errors in M_V^{HB} . The values of column r_{Harris} are taken from Harris (1996). Distances in kpc, brightness in mag.

5.4. Masses

To classify the clusters according to Burkert & Smith (1997), we have to determine the masses from the total absolute brightnesses. Because we could not measure the apparent total brightness, we used the values given by Harris (1996). With the extinctions and distance moduli given above (Table 8), we get the absolute total brightnesses via

$$M_V^{total} = V^{total} - A_V - (m - M)_0 \quad (7)$$

We determined the masses using a mass-to-light-ratio of $(\frac{M}{L})_V = 3$ (Chernoff & Djorgovski 1989). Table 10 shows the results. Thus, NGC 6441 is one of the most massive clusters of the galaxy. ω Cen/NGC 5139 has $\log(M/M_\odot) = 6.51$ (Harris 1996).

NGC	V^{total}	M_V^{total}	$\log\left(\frac{M}{M_\odot}\right)$
5927	8.01	-7.52	5.42
6316	8.43	-8.28	5.72
6342	9.66	-6.07	4.85
6441	7.15	-9.61	6.26
6760	8.88	-7.48	5.41
6528	9.60	-6.65	5.07
6553	8.06	-7.65	5.47

Table 10. Absolute total brightnesses and masses for all clusters. The apparent brightnesses were taken from Harris (1996).

6. Classification and assignment

After having determined the parameters of our cluster sample, we now discuss each cluster's possible affiliations with the galactic structure components i.e. halo, disk or bulge for each cluster. The necessary criteria are introduced in the following subsection.

6.1. The assignment criteria

6.1.1. Disk and Halo: Zinn (1985)

Zinn (1985) divided the GC-system into a metal-poor ($[M/H] \leq -0.8$ dex) halo- and a metal-rich ($[M/H] \geq -0.8$) disk-subsystem. This distinction also correlated with the kinematics and spatial distribution of their objects. The resulting criteria are listed in Table 11. Equation 8 gives the orbital velocity v_c of a cluster depending on its observed radial velocity v_{rad} . v_c can be compared to the net rotation as given in Table 11.

6.1.2. Bulge and (thick) disk: Minniti (1995,1996)

Minniti (1995, 1996) divided Zinn's metal-rich disk system further into GCs belonging to the (thick) disk on the one

hand and to the bulge on the other. Comparing the GCs with their corresponding field population, he assigned the GCs with galactocentric distances $R_{gc} \leq 3$ kpc to the bulge and the ones with $R_{gc} \geq 3$ kpc to the thick disk.

6.1.3. Inner halo, bar and disk: Burkert & Smith

Burkert & Smith (1997) used the masses of the metal-rich GCs to distinguish between a group belonging to the inner halo and a group which can be further divided into a bar- and a ring-system using the kinematics and spatial distribution of the clusters (see Table 12).

6.1.4. Radial velocities

Unfortunately, there do not exist any data on proper motions of our clusters. The only kinematic information available are radial velocities, catalogued by Harris (1996). Thus, we can only check, whether a disk orbit is compatible with a given radial velocity. This is possible by comparing the measured radial velocity v_{rad} with the expected one, calculated via equation 8 assuming that disk clusters move on circular orbits in the galactic plane.

$$v_{rad} = v_c \sin\left(l + \arctan\left(\frac{y}{R_s - x}\right)\right) - v_s \sin(l), \quad (8)$$

where l is the galactic longitude, and x and y are the heliocentric coordinates. We used $R_s = 8.0$ kpc and $v_s = 220$ km/s. v_c gives the velocities of the clusters in the plane, corresponding to the galactic rotational velocity $v_{rot}(R_s - x)$ with the values taken from Fich & Tremaine (1991).

6.1.5. Metallicity gradient

The metallicity gradient of the disk is an uncertain criteria insofar, as it is defined for the outer ranges of the

subsystem	$[M/H] \leq -0.8$ dex	$[M/H] \geq -0.8$ dex
v_{rot} [km/s]	50 ± 23	152 ± 29
σ_{rot} [km/s]	114	71

Table 11. Kinematics and spatial distribution of the metal-rich and -poor subsystems of GCs according to Zinn (1985)

group	inner halo	bar	disk
$\log(M/M_s)$	≥ 5.55	≤ 5.55	≤ 5.55
v_{rot} [km/s]	24 ± 23	24 ± 23	164 ± 6
v_{rot}/σ_{rot}	0.3	0.3	6
spatial distribution	concentrated to center	bar-like structure	$(4 \leq R_{gc} \leq 6)$ kpc

Table 12. Criteria for subgroups of the metal-rich GCs according to Burkert & Smith (1997).

galactic disk. We use a metallicity gradient referring to the population of old open clusters. The oldest of these objects have ages similar to the youngest GCs (Phelps et al. 1994). Their scale height is comparable to other thick disk objects. Assuming that they are related to a possible disk population of GCs (Friel 1995), we can use their metallicity gradient

$$\frac{\partial[\text{Fe}/\text{H}]}{\partial R_{gc}} = -0.091 \pm 0.014 \quad (9)$$

(Friel 1995) as a criterion for whether our GCs belong to the galactic thick disk or not.

6.2. The assignment

Using the above criteria, we assigned the clusters of our sample according to Table 13. The values of the parameters necessary to decide on group membership are listed in Table 14.

NGC	Zinn	Minniti	Burkert	v_{rad}^{disk}	$\partial_r[\text{M}/\text{H}]$
5927	d	(d)	d	+d	-d
6316	?	?	bu	+d	-d
6342	?	bu	ba	-d	-d
6441	?	?	bu	-d	-d
6760	d	?	d	-d	-d
6528	?	bu	ba	-d	-d
6553	(h)	bu	ba	-d	-d

Table 13. Assignment of the clusters to the systems **disk**, **halo**, **bulge** and **bar** according to the criteria in the first column. ? is used if no assignment is possible, the symbols d, h, bu and ba together with + or - relate to criteria which only can decide whether an object belongs to a certain group or not. Symbols in brackets denote uncertainties explained in the text.

As for the metallicities of our clusters, they all belong to the disk system according to Zinn, which is obvious as the sample had been selected in this way. Not so obvious is the comparison with the net rotation of Zinn’s disk group. Only NGC 5927 shows a value of v_{rot} which is not totally off the net rotation as given in Table 11.

The clusters belonging to the bulge according to Minniti’s criterion are members of the bar following the arguments of Burkert & Smith (1997). Binney et al. (1997) quote a value of 20° for the angle between x-axis in galactocentric coordinates and the major semiaxis of the bulge structure. Its end lying nearer to the sun is located at small galactic longitudes ($y \leq 0$ in cartesian coordinates). Fig 34 shows the spatial distribution of our cluster sample. The coordinates of the ‘bar’ clusters NGC 6342, 6528 and 6553 according to Burkert & Smith seem to be consistent with a structure described by Binney et al. (1997). However, as the referee pointed out, we do not know how

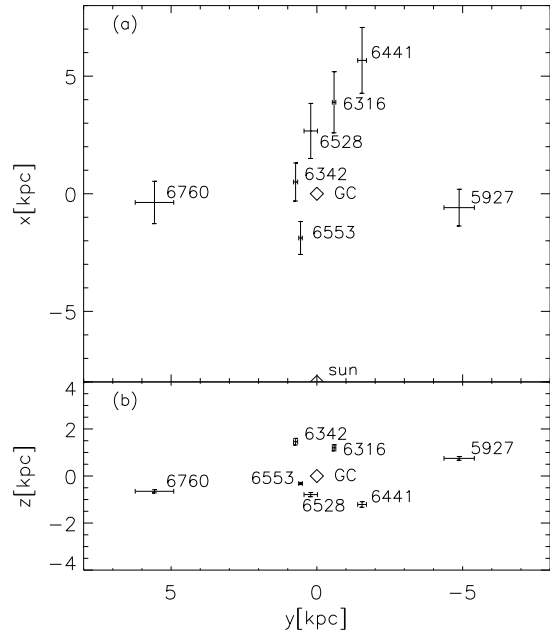


Fig. 34. Distribution of the cluster sample in the galactocentric x-y-plane (a) and y-z-plane (b). In the upper panel, the observer is located at $z \geq 0$. The distribution in the y-z-plane is as seen from the sun. The distances used correspond to r_{rel} in Table 9.

long-lived the Milky-Way bar is, and other tracers of old populations such as RR Lyrae do not follow the bar (Alcock et al. 1998). Moreover, the distance between the ‘bar’ clusters NGC 6528 and NGC 6553 is about 5 kpc, which is much larger than the length of the Milky-Way bar according to most authors (e.g. Binney et al. 1997). Also note in Fig 34, that the errors in the x-coordinate are larger than those in y and z.

There are only two ‘disk’ clusters remaining, assuming Burkert & Smith’s definition of disk clusters: NGC 5927 and NGC 6760. However, the radial velocities corroborate this result for NGC 5927 only. For any other cluster, the radial velocities seem to exclude an assignment to the disk.

The metallicity gradient of the old open clusters leads to the conclusion that none of our clusters is to be assigned to the thick disk. Taken the whole sample of metal rich clusters (i.e. clusters with $[\text{M}/\text{H}] \geq -0.8$ dex according to Zinn 1985, see Tables 16, 15), we find only three objects, which could be disk clusters according to the metallicity gradient criterium.

Some of the clusters do not meet any of the criteria. Interestingly, they are the most massive, but metal-poorest objects of the sample. These objects are NGC 6316, 6760, and 6441 as well as (in Table 16) NGC 104, 6356 and 6388. Although NGC 104 seems to be a disk cluster and mostly is referred to as such, the large distance to the galactic plane (3 kpc) does not support this assignment. Probably, the mentioned objects belong to the halo, be-

NGC	5927	6316	6342	6441	6760	6528	6553
[M/H][dex]	-0.29	-0.60	-0.42	-0.39	-0.57	0.00	-0.04
R_{gc} [kpc]	5.0	4.1	1.7	6.1	5.6	2.8	2.0
z [kpc]	0.8	1.3	1.6	-1.3	-0.7	-0.8	-0.3
$\log(M/M_{\odot})$	5.42	5.72	4.84	6.26	5.41	5.07	5.47
v_{rot} [km/s]	220	220	210	225	220	195	210
v_{rad} [km/s]	-116	72	81	18	-28	185	-7
v_{rot}^{disk} [km/s]	265	-308	114	18	121	1910	37
v_{rad}^{disk} [km/s]	-75	-32	164	-58	56	15	58
$[M/H]_{oc}(r)$ [dex]	0.18	0.20	0.46	0.01	0.11	0.33	0.51

Table 14. All relevant parameters for the assignment. [M/H] gives the metallicity according to the [M/H] – ΔV -relation, R_S the heliocentric distance, R_{gc} the galactocentric distance and z the distance to the disk. The M in $\log(M/M_{\odot})$ stands for cluster mass, v_{rot} for the orbital velocity, derived via the rotational velocity curve of Fich & Tremaine (1991), v_{rad} for the observed radial velocity and v_{rot}^{disk} for the orbital velocity of the clusters, calculated using v_{rad} and the assumption of circular cluster orbits (in order to compare with a net rotation). v_{rad}^{disk} contains the expected radial velocity assuming disk orbits and $[M/H]_{oc}(r)$ the values derived via a metallicity gradient of the old open clusters (Friel 1995).

Name	R_{gc}	z	[M/H]	v_{rad}	v_{rad}^{disk}	$\log(M/M_{\odot})$	v_{rot}^{disk}	$[M/H]_{oc}$
NGC 104	7.3	-3.0	-0.76	-19	-26	6.16	202	0.06
Lynga 7	4.2	-0.3	-0.62	8	-95		106	0.35
NGC 6256	2.3	0.5	-0.70			4.87		0.52
NGC 6304	2.2	0.6	-0.59	-107	-38	5.32	478	0.52
NGC 6356	7.0	2.6	-0.50	27	-56	5.81	-361	0.09
NGC 6352	3.3	-0.7	-0.70	-121	-93	4.99	244	0.42
Ter 2	1.6	0.4	-0.25	109	79	4.41	305	0.58
Liller 1	2.6	0.0	0.22	53	73	5.45	127	0.49
Ter 1	1.5	0.1	-0.35	35	-40	3.71	-108	0.59
Ton 2	1.4	-0.5	-0.50			4.84		0.60
NGC 6388	4.4	-1.4	-0.60	81	155	6.32	54	0.32
Pal 6	1.4	0.2	-0.10	201	31	5.34	1112	0.60
Ter 5	0.6	0.2	-0.28	-94		5.56		0.67
NGC 6440	1.2	0.5	-0.34	-79	180	5.89	-49	0.62
Ter 6	0.6	-0.3	-0.65	126	-77	5.14	-305	0.67
NGC 6496	4.4	-2.0	-0.64	113	136	5.28	-364	0.32
Ter 10	0.8	-0.3	-0.70			5.52		0.66
NGC 6539	3.0	0.9	-0.66	-45	130	5.71	32	0.46
NGC 6624	1.2	-1.1	-0.42	53	181	5.39	71	0.62
NGC 6637	1.5	-1.5	-0.71	40	-191	5.40	-52	0.59
Pal 8	5.2	-1.5	-0.48	-43	-134	4.60	-27	0.26
Pal 10	6.4	0.3	-0.10			4.71		0.14
Pal 11	7.6	-3.4	-0.39	-68	-24	5.11	-72	0.04
NGC 6838	6.7	-0.3	-0.73	-23	25	4.62	161	0.12

Table 15. The relevant parameters of the remaining metal rich GCs according to Harris (1996). The columns are labeled as in Table 14. Distances are given in kpc, metallicities in dex and velocities in km/s.

ing its metal-richest clusters. Zinn (1985) and Armandroff (1993) point to the fact that the division into metal-rich and poor clusters is by no means an exact one, but that there is a metal-rich sample of halo clusters as well as a metal-poorer one of disk objects. Richtler et al. (1994) discussed the existence of a subgroup of disk clusters according to Zinn (1985), based on an analysis of the metallicities and the minimum inclination angles derived from z/R_{gc} -

values for these clusters. They conclude that the clusters NGC 6496, 6624 and 6637 might not be disk clusters after all, but belong to the halo. Adding their argument to the above discussion, we end up with 3 probable disk members (NGC 5927, additionally from Table 16 Liller 1 and Pal 10. Pal 11 is excluded because of its large minimum inclination angle.) and 9 clusters (NGC 104, 6316, 6356, 6388, 6441, 6496, 6624, 6637 and 6760) that more likely

Name	Zinn	Minniti	Burkert	v_{rad}	$[M/H]_{oc}$
NGC 104	d	-	?	+d	-d
Lynga 7	d	-	-	-d	-d
NGC 6256	-	bu	ba	-d	-d
NGC 6304	?	bu	ba	-d	-d
NGC 6356	?	-	?	-d	-d
NGC 6352	?	-	ba	+d	-d
Ter 2	?	bu	ba	+d	-d
Liller 1	d	bu	ba(d)	+d	+d
Ter 1	?	bu	ba	-d	-d
Ton 2	?	bu	ba	-	-d
NGC 6388	d	-	?	d?	-d
Pal 6	?(bu)	bu	ba	-d	-d
Ter 5	-	bu	bu	-	-d
NGC 6440	?	bu	bu	-d	-d
Ter 6	?	bu	bu	-d	-d
NGC 6496	?	-	ba	+d	-d
Ter 10	?	bu	ba	-	-d
NGC 6539	?	bu?	bu	-d	-d
NGC 6624	?	bu	ba	-d	-d
NGC 6637	?	bu	ba	-d	-d
Pal 8	?	-	d	-d	-d
Pal 10	-	-(d)	d	-	+d
Pal 11	?	?	d	d?	+d?
NGC 6838	d	-	d	-d	-d

Table 16. Suggested assignment according to the criteria discussed above for the remaining metal rich GCs. The columns are labeled as in Table 13.

belong to the halo than to the (thick) disk. The rest of the clusters (NGC 6342, 6528, 6553 and the remaining ones of Table 16) fall in with the bulge/bar-group of Minniti (1995) and Burkert & Smith (1997).

7. Conclusions

We derived the parameters for five GCs near the galactic center in a uniform manner, employing a new calibration of methods which relate structures in the CMDs with the parameters. Taking into account the differential reddening and correcting the CMDs for it leads to more accurately determined parameters and a decreasing absolute reddening. There might be a systematic effect on distances, if the differential reddening is not taken care of.

With the $[M/H] - \Delta V$ - method we present a accurate way to estimate differentially metallicities of metal-rich GCs. Especially it might prove useful for surveys of clusters in V, V-I, as their CMDs only need to contain the HB and turnover of the AGB/RGB.

The metallicities of our program clusters all lie in the range of the clusters constituting the classical disk-system of GCs in the Milky Way. However, different criteria defining subgroups of the GC-system partly lead to differing results. Most of the metal-rich GCs seem to belong to a bar/bulge-structure, and only a minority could clearly be addressed as 'disk'-clusters. So the classical disk-system is

more likely to be a mixture between a halo- and bulge-component.

Acknowledgements. We are indebted to E.K. Grebel for the most interesting and valuable discussions, especially on the technique of differential dereddening. We would like to thank the referee D. Minniti for helpful comments and criticism.

References

- Alcock, C., Allsman, R.A., Alves, D.R. et al. 1998, ApJ 492, 190
- Armandroff, T.E. 1988, AJ 96, 588
- Armandroff, T.E., Zinn, R. 1988, AJ 96, 92
- Armandroff, T.E. 1989, AJ 97, 375
- Armandroff, T.E. 1993, ASP Conf. Ser. 48, 48
- Bertelli, G., Bressan, A. Chiosi, C. et al. 1994, A&AS 106, 275
- Binney, J., Gerhard, O., Spergel, D. 1997, MNRAS 288, 365
- Burkert, A., Smith, G.H. 1997, ApJ 474, L15
- Caretta, E., Bragaglia, A. 1998, A&A 329, 937
- Caretta, E., Gratton, R., Fusi Pecci, F., Clementini, G. 1998, *in preparation*
- Chernoff, D.F., Djorgovski, S. 1989, ApJ 339, 904
- Davidge, T.J., Harris, W.E., Bridges, T.J. et al. 1992, ApJS 81, 251
- Deutsch, E.W. 1996, BAAS 189, 44.06
- Fich, M., Tremaine, S. 1991, ARAA 29, 409
- François, P. 1991, A&A 274, 56
- Friel, E.D. 1995, ARAA 33, 381
- Fullton, L.K. 1996, ASP Conf. Ser. 92, 269, eds. H. Morrison, A. Sarajedini
- Garnavich, P.M., Vandenberg, D.A., Zurek, D.R. et al. 1994, AJ 107, 1097
- Gieren, W. P., Richtler, T., Hilker, M., 1994, ApJ 433, L73
- Gieren, W. P., Fouqué, P., Gómez, M., 1998, ApJ 496, 17
- Grebel, E.K., Brandner, W., Richtler, T. et al. 1995, BAAS 187, 8203
- Grebel, E.K., Roberts, W. 1995, A&AS 109, 293
- Guarnieri, M.D., Ortolani, S. Montegriffo, P. et al. 1998, A&A 331, 70
- Harris, W.E. 1996, AJ 112, 148
- Heitsch, F., Richtler, T. 1999, *in preparation*
- Hesser, J.E., Hartwick, F.D.A. 1976, ApJ 203, 97
- Hesser, J.E., Harris, W.E., Vandenberg, D.A. et al. 1987, PASP 99, 739
- Holtzman J.A., Burrows, C.J., Casertano, S. et al. 1995, PASP 107, 1065
- Meyer, D.M., Savage, B.D. 1981, ApJ 248, 545
- Minniti, D. 1995, AJ 109, 1663
- Minniti, D. 1996, ApJ 459, 175
- Montgomery, K.A., Marschall, L.A., Janes, K.A. 1993, AJ 106, 181
- Olszewski, E.W., Schommer, R.A., Suntzeff, N.B., Harris, H.C. 1991, AJ 101, 515
- Ortolani, S., Barbuy, B., Bica, E. 1990, A&A 236, 362
- Ortolani, S., Bica, E., Barbuy, B. 1992, A&A 92, 441
- Ortolani, S., Bica, E., Barbuy, B. 1997, A&A 326, 614
- Phelps, R.L., Janes, K.A., Montgomery, K.A. 1994, AJ 107, 1079
- Rich, R.M., Sosin, C., Djorgovski, S.G. et al. 1997, ApJ 484, L25

- Richtler, T., Grebel, E.K., Seggewiss, W. 1994, *A&A* 290, 412
- Richtler, T., Grebel, E.K., Subramaniam, A. et al. 1998, *A&AS* 127, 167
- Sagar, R. Subramaniam, A., Richtler, T. 1998, *preprint*
- Samus, N., Kravtsov, V., Ipatov, A. et al. 1996, *A&AS* 119, 191
- Sarajedini, A. 1994, *AJ* 107, 618
- Sarajedini, A., Norris J.E. 1994, *ApJS* 93, 161
- Savage, B., Mathis, J. 1979, *ARAA* 17, 73
- Stetson, P.B. 1987, *PASP* 99, 191
- Stetson, P.B. 1992, *JRASC* 86, 71
- Stetson, P.B., VandenBerg, D.A., Bolte, M. 1996, *PASP*, 108, 560
- Tanvir, N.R. 1996, Cepheids as distance indicators, in: *The Extragalactic Distance Scale*, Symp.Ser.10, STScI, Cambridge University Press
- Turner, D.G. 1994, *RMAA* 29, 163
- Walker, A. R. 1992, *ApJ* 390, L81
- Zinn, R. 1985, *ApJ* 293, 424